

Extension of the PLANETOCOSMICS framework for the calculation of geomagnetic cutoff histograms

Lukas Hennig

May 31, 2022

Abstract

Geomagnetic cutoff rigidities, or cutoffs for short, are physical quantities used in the context of the access problem. The latter describes the problem of determining whether charged cosmic ray particles can reach an arbitrary but fixed point in the magnetosphere or whether their trajectories are bent away by Earth's magnetic field. Previous studies related to the computation and further application of these cutoff rigidities were done by von Doetinchem and Yamashiro[1], who used the PLANETOCOSMICS framework to calculate the cutoffs. One of their findings was the appearance of several regions close to Earth's poles with remarkably high cutoffs, which is unexpected because cutoffs typically decrease the farther one travels away from the equator. It was not clear whether these cutoff hotspots resulted from a real phenomenon or a bug in the software. This work starts with a short introduction discussing the access problem and the PLANETOCOSMICS framework, followed by an explanation of the origin of these cutoff hotspots, which appeared as the result of a mistake in the PLANETOCOSMICS input scripts. Additionally, this work proposes an algorithm for calculating so-called cutoff histograms. This algorithm lifts some problems encountered during the use of PLANETOCOSMICS's default algorithm. Examples of cutoff histograms calculated at different points in the magnetosphere are presented and discussed in the end.

This project was carried out in collaboration with Professor Philip von Doetinchem and his working group at the University of Hawai'i at Mānoa. It was financially supported by the *Deutscher Akademischer Austauschdienst* through the *RISE Worldwide*¹ program.

Contents

- 1. Introduction** **3**
 - 1.1. Definition and use of the rigidity 3
 - 1.2. Discussion of the access problem 5
 - 1.2.1. The first period: Theoretical considerations and results 6
 - 1.2.2. The second period: Using digital computers for cutoff calculations 8
 - 1.3. The PLANETOCOSMICS simulation framework 11

- 2. Finding the origins of the geomagnetic cutoff hotspot** **13**
 - 2.1. Description of the original draft 13
 - 2.2. Determining whether the hotspot is a real phenomenon 16
 - 2.3. Finding the source of the bug 18

- 3. Extending the PLANETOCOSMICS framework** **21**
 - 3.1. Motivation for the extension 22
 - 3.2. Sketching the new algorithm 25
 - 3.3. The syntax of the new macro 26
 - 3.4. Examples of cutoff histograms 27

- 4. Summary and results** **30**

- Appendix** **32**
 - A. Example macro file for PLANETOCOSMICS** **32**

¹<https://www.daad.de/rise/en/rise-worldwide/>

1. Introduction

1.1. Definition and use of the rigidity

The rigidity of a particle is a physical quantity especially useful in the study of particle trajectories in the presence of a stationary magnetic field. It is defined as

$$R = \frac{pc}{|q|} \quad (1)$$

where p is the magnitude of the particle's momentum vector $p = |\vec{\mathbf{p}}|$, c is the speed of light, and q is the particle's electric charge. If we consider two particles that are both either positively or negatively charged starting their trajectory through a stationary magnetic field at the same initial position and with the same initial direction, then the implication

$$R_1 = R_2 \implies \exists \sigma(t) : \vec{\mathbf{r}}_2(t) = \vec{\mathbf{r}}_1(\sigma(t)) \quad (2)$$

holds. In the above statement, $R_{1/2}$ are the particles' rigidities, $\vec{\mathbf{r}}_{1/2}(t)$ are the particles' trajectories, and $\sigma(t) : \mathbb{R} \rightarrow \mathbb{R}$, $t \mapsto \sigma(t)$ maps time t to a possibly different time $t' = \sigma(t)$. This statement expresses that, given the stated prerequisites, any two particles with the same rigidity will move along the same trajectory through the magnetic field. Note that the particles will generally not move along that trajectory with the same velocity. This is represented in the above statement by the appearance of $\sigma(t)$: if particle 2 is at point $\vec{\mathbf{r}}_2(t)$ at time t , then the statement says that particle 1 was (or will be) at the same point $\vec{\mathbf{r}}_1(t')$ at a different time $t' = \sigma(t)$.

This property will be used extensively for the rest of this project. Instead of studying the trajectories of particles through a magnetic field as a function of energy, momentum, and charge, it is sufficient to study them as a function of rigidity.

Mathematically, $\vec{\mathbf{r}}_2(t)$ and $\vec{\mathbf{r}}_1(\sigma(t))$ are just two different parametrizations of the same curve. Any curve can be arbitrarily reparametrized, but it will still represent the same mathematical object. To remove this ambiguity, a curve can be naturally parametrized by its arc length

$$s(t) = \int \sqrt{d\vec{\mathbf{r}} \cdot d\vec{\mathbf{r}}} = \int_0^t \left| \frac{d\vec{\mathbf{r}}(t')}{dt'} \right| dt' = \int_0^t |\vec{\mathbf{v}}(t')| dt'. \quad (3)$$

Statement 2 can easily be proven with the help of the arc length. We start by looking at the equations of motion of a particle in a magnetic field in special relativity,

$$\dot{\vec{r}}(t) = \vec{v}(t) \quad (4)$$

$$\dot{\vec{p}}(t) = q \cdot \vec{v}(t) \times \vec{B}(\vec{r}(t)), \quad (5)$$

where $\vec{p}(t)$ is the relativistic momentum,

$$\vec{p}(t) = \gamma(v(t)) m \vec{v}(t), \quad (6)$$

with $v(t) = |\vec{v}(t)|$, and (t, \vec{r}) are the time and position in our arbitrary but fixed inertial frame. After carrying out the time derivative of the relativistic momentum, we obtain

$$\frac{d\vec{p}(t)}{dt} = \gamma(v(t))^3 m \dot{\vec{v}}_{\parallel} + \gamma(v(t)) m \dot{\vec{v}}_{\perp}, \quad (7)$$

where $\dot{\vec{v}}_{\parallel}$ and $\dot{\vec{v}}_{\perp}$ are the components of the acceleration parallel/perpendicular to the velocity $\vec{v}(t)$.

By inserting eq. (7) in the left side of eq. (5), and by using that the right side of eq. (5) is perpendicular to the velocity $\vec{v}(t)$ due to the cross product, we obtain the equations

$$\gamma(v(t)) m \dot{\vec{v}}_{\perp} = q \cdot \vec{v}(t) \times \vec{B}(\vec{r}(t)) \quad (8)$$

$$\gamma(v(t))^3 m \dot{\vec{v}}_{\parallel} = 0. \quad (9)$$

Equation (9) shows that the acceleration of the particle caused by the magnetic field will always be perpendicular to the velocity $\vec{v}(t)$. This implies that the speed $v(t) = \sqrt{\vec{v}(t) \cdot \vec{v}(t)}$ is constant over time since

$$\frac{dv(t)}{dt} = \frac{\dot{\vec{v}}(t) \cdot \vec{v}(t)}{v(t)} = 0. \quad (10)$$

This holds because $\dot{\vec{v}}(t) \cdot \vec{v}(t) = 0$ in our case. With this result, we can go back to eq. (3). If we denote the constant velocity of the particle by v_0 , then we get

$$s(t) = \int_0^t |\vec{v}(t')| dt' = \int_0^t v_0 dt' = v_0 t. \quad (11)$$

Now we can reparametrize eq. (8) which will yield the proof of statement 2. Let us reparametrize $\vec{r}(t)$ by defining the curve

$$\vec{u}(s) = \vec{r}\left(\frac{s}{v_0}\right) = \vec{r}(t). \quad (12)$$

By expressing eq. (8) with $\vec{\mathbf{u}}(s)$, we obtain

$$\frac{d^2}{dt^2} \vec{\mathbf{u}}(s) = \frac{q}{\gamma m} \frac{d\vec{\mathbf{u}}(s)}{dt} \times \vec{\mathbf{B}}(\vec{\mathbf{u}}(s)). \quad (13)$$

Finally, we use that $\frac{d}{dt} = v_0 \frac{d}{ds}$ to get

$$\ddot{\vec{\mathbf{u}}}(s) = \text{sgn}(q) \frac{c}{R} \dot{\vec{\mathbf{u}}}(s) \times \vec{\mathbf{B}}(\vec{\mathbf{u}}(s)), \quad (14)$$

where c is the speed of light, and R is the rigidity as defined in eq. (1). This equation shows us that any two particles with the same rigidity and an equal sign of the charge will follow the same equation of motion in the chosen parametrization. Therefore, they will have the same trajectories if they start at the same position and with the same initial direction.

1.2. Discussion of the access problem

During this project, we want to develop methods to better understand the access that cosmic ray particles, starting from infinity, have to different points in the magnetosphere. This problem will subsequently be named the ‘‘access problem’’. In this context, cutoff rigidities have proven themselves very useful for describing different phenomena that will be discussed in this section.

The terminology used in the research of geomagnetic cutoff rigidities experienced some ambiguities and confusion throughout its history. A summary of this can be found in Cooke *et al.*[2] that we will discuss briefly in the following, together with suggestions for more unambiguous definitions that we will use throughout this project and that will be explained in this section. The article discusses two main periods into which the research on cutoff rigidities can be divided historically. The first period started in the 1930s with the work of Størmer, Bouckaert, Lemaitre, and Vallarta[3]–[7]. They used purely theoretical considerations to gain insight into the access of cosmic rays to points in the geomagnetic field. Starting in the 1960s, the advent of digital computers allowed the calculation of the trajectories of particles through the geomagnetic field numerically, which allowed researchers to gain more insight into the different kinds of trajectories that cosmic rays follow along their journey. Although we will mainly use the methods and the terminology established in the latter period, we will nevertheless discuss the first period briefly to gain a more solid understanding of the problem.

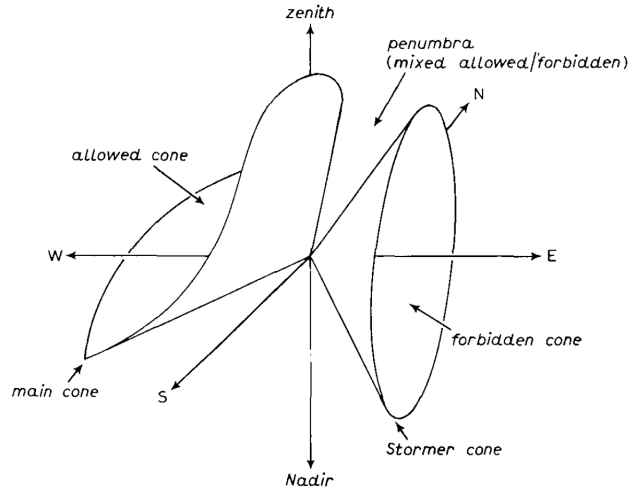


Figure 1: An example of how the different cones and the penumbra could look like at a point in the magnetosphere and for a fixed rigidity R . Note that the forbidden cone is a right circular cone, while the allowed cone is a solid angle region that does not necessarily have to be a cone in the mathematical sense. Source: Cooke *et al.*[2]

1.2.1. The first period: Theoretical considerations and results

The magnetic field produced by currents inside the Earth can approximately be described as a magnetic dipole field. As Cooke *et al.*[2] explain, this approximation is handy because Carl Størmer[3], [8] showed that for any point in a magnetic dipole field and a chosen fixed rigidity R , there exists a right circular conical shell of directions within which all directions are inaccessible for particles starting from infinity with rigidities smaller than R . The opening angle of this cone increases with decreasing R , and vice versa. The latter is intuitive since particles with high rigidities travel through the geomagnetic field without a significant bending of their trajectory. In contrast, particles with smaller rigidities are shielded stronger by the magnetic field. This right circular conical shell is often called “Størmer cone”. The Størmer cone is the surface of the so-called “forbidden cone”, which is a solid cone consisting of directions inaccessible for particles with rigidities smaller than R . Both cones are depicted, among other quantities that we will talk about soon, in fig. 1.

So far, we only used a point of view which was named the “direction picture” by Cooke *et al.*[2]. In this picture, we fix a point in the magnetosphere and a rigidity R , and we

are interested in all the directions in which a particle with rigidity R could or could not arrive. The directions in which a particle could arrive are called “allowed directions”, while the other ones are called “forbidden”.

To define the so-called “Størmer cutoff rigidity”, we have to adapt another point of view named the “rigidity picture”. In this picture, we choose a point in the magnetosphere and a fixed direction, and then we calculate particle access as a function of rigidity. If one chooses a point in space and a direction, one can show that there exists a rigidity R_S such that the Størmer cone lies in that direction. Furthermore, for all rigidities smaller than R_S , the trajectories are also forbidden since they lie in the forbidden cone then. The rigidity R_S is called the “Størmer cutoff rigidity”, or “Størmer cutoff” for short.

The existence of the forbidden cone is purely a property of the magnetic dipole field. So far, we did not include the solid Earth and its atmosphere in our model. It turns out that these are very important for the determination of allowed and forbidden directions because trajectories crossing the Earth and its lower atmosphere will get lost in their interactions with the nuclei of the Earth and the atmosphere, resulting in more forbidden directions.

Cooke *et al.*[2] explain further that Lemaitre and Vallarta[6], [7] treated this more complex problem when they searched for regions of allowed directions at fixed rigidities, i.e., in the direction picture. They realized that, in the absence of the solid Earth, all trajectories asymptotic to the simplest bound periodic orbits form the surface of a cone. All directions inside that cone are accessible from infinity if the solid Earth is not considered. To include the effect of the solid Earth, one can additionally mark all directions that are at least once tangential to the surface of the Earth, forming another cone. The set of trajectories within both cones forms another cone of trajectories allowed by both restrictions. The surface of the latter cone is named the “main cone”, while the solid cone of allowed directions is called the “allowed cone”. It has to be mentioned that the word *cone* is a bit misleading at this point since the main cone can be a complicated surface that could even be split into two separate cones. Both the main cone as well as the allowed cone are depicted in fig. 1.

A second cutoff rigidity can be defined due to the main cone, where we use the rigidity picture again. If we fix a point in space and a direction, there will be a rigidity value such that the main cone lies in that fixed direction. This rigidity value is called “main cone cutoff rigidity”. For larger rigidities, the main cone widens, and the direction will be

included in the allowed cone. This is rather intuitive since a particle with a high enough rigidity will not be bent much by the magnetic field, entering the point from infinity in a straight line for the extreme case of rigidity $R \rightarrow \infty$. At this point, we implicitly assumed that the fixed direction points above the local horizon. We will discuss this assumption in more detail later.

The directions that are neither in the allowed cone nor the forbidden cone belong to the so-called “penumbra” (see fig. 1). The penumbra consists of allowed as well as forbidden directions. As Cooke *et al.*[2] explain, the structure of allowed and forbidden bands in the penumbra are very complex, and deeper investigations were only possible due to the advent of digital computers.

1.2.2. The second period: Using digital computers for cutoff calculations

The advent of digital computers allowed researchers to calculate the trajectories of particles through the geomagnetic field in a time-efficient manner. As Cooke *et al.*[2] explain, each trajectory is not calculated starting from infinity until it reaches its destination. Instead, one fixes a point in space, a direction, and a rigidity and then calculates the trajectory of a particle with the opposite charge by numerically integrating the equation of motion (e.g., eq. (8) or 14). This method is physically equivalent to tracing the particle going back in time through the magnetic field. If the particle escapes the magnetosphere, we call this trajectory allowed. On the other hand, if the particle intersects the Earth or is trapped in a periodic orbit, this trajectory is forbidden because no particle starting at infinity could traverse that path in the reverse direction. Note that this procedure uses the rigidity picture, while the theoretical considerations in the first period focused on the direction picture.

If we want to integrate the equation of motion numerically, we must be able to calculate realistic values for the magnetic field $\vec{\mathbf{B}}(\vec{\mathbf{r}})$. There are different models that one can use for this task, and we will discuss some of them later in section 1.3 during the introduction of the PLANETOCOSMICS simulation framework.

The procedure to trace back a particle described above needs a position, a direction, and a rigidity as input, and it will tell us whether the trajectory is allowed or forbidden. To gain a more complete picture of the structure of allowed and forbidden trajectories for different rigidities, directions, and points in space, one typically chooses a grid of

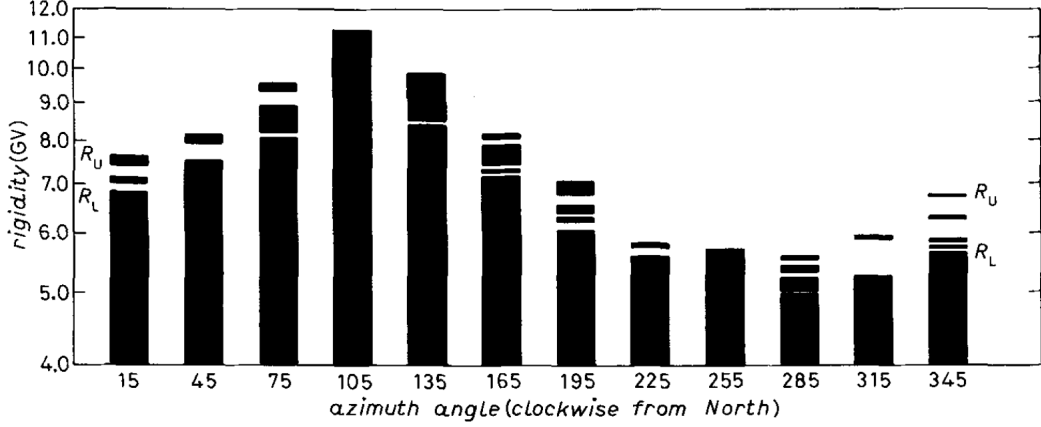


Figure 2: The result of tracing back particles from the location 20°N, 270°E, 400 km altitude at a zenith angle of 60°. The trajectories were calculated at 1% rigidity spacing intervals and every 30° in the azimuth angle. Forbidden trajectories are indicated as black while allowed ones are white. The highest *computed* forbidden→allowed transition is indicated as R_U while the lowest is named R_L . Source: Cooke *et al.*[2]

parameters on which this method is applied. One concrete example of this is shown in fig. 2, where the fixed parameters are the position and the zenith angle, while the azimuth and the rigidity are chosen from a grid of parameters on which the procedure to trace back particles is applied.

As Cooke *et al.*[2] point out, the rigidity corresponding to the highest and lowest *computed* forbidden→allowed transitions are not, in general, the main and the Størmer cutoff rigidity. This is an unavoidable consequence of using a discrete rigidity grid rather than a continuous spectrum like for theoretical considerations. The highest and lowest forbidden→allowed transition could be in a band which is too narrow to be detected by our discrete rigidity grid. Hence, to avoid confusion, we call the rigidities associated with the highest and lowest *computed* forbidden→allowed transitions R_U and R_L , respectively. These quantities are related to the main cutoff R_M and the Størmer cutoff R_S by the inequations

$$R_U \leq R_M \quad (15)$$

$$R_L \geq R_S. \quad (16)$$

Cooke *et al.*[2] additionally define a so-called *effective cutoff rigidity* R_C that contains

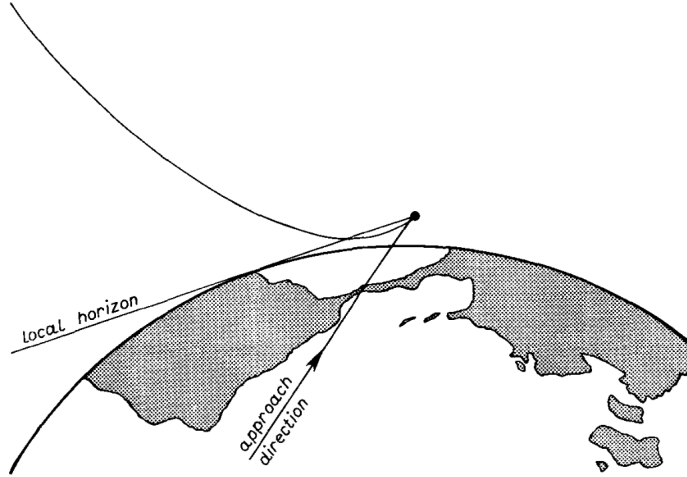


Figure 3: Sketch of an example trajectory that is allowed although its approach direction is below the local horizon. Source: Cooke *et al.*[2]

information about R_L , R_U , and the penumbral structure. It satisfies the inequality $R_L \leq R_C \leq R_U$. If we use linear weighting and uniformly spaced rigidity intervals ΔR , the effective cutoff R_C is defined as

$$R_C = R_U - n_{\text{allowed}} \cdot \Delta R, \quad (17)$$

where n_{allowed} is the number of allowed rigidities found in the penumbra, i.e., between R_L and R_U .

In fig. 2, we can see that there are no forbidden \rightarrow allowed or allowed \rightarrow forbidden detected for rigidities R with $R > R_U$. This makes sense intuitively: if a particle has a large rigidity, its trajectory should be less bent by the magnetic field than the trajectory of a particle with a smaller rigidity. In the extreme case of $R \rightarrow \infty$, we even would expect the particle to be traced back in a straight line towards infinity. Up to this point, we made an implicit assumption: the direction in which the particle will be traced back must be over the local horizon of that point in space. The local horizon at a particular point in space is the surface of the solid cone generated by connecting said point with all points on Earth that are visible from that point. This is illustrated in fig. 3 where the local horizon for one particular direction is sketched. If we trace back a particle in a direction below the horizon, large rigidities will lead to forbidden trajectories since the particles would intersect with the Earth. At first, one could suspect that there may be no allowed trajectories if we start from a direction below the local horizon, but this

would be false. In fact, e.g., Humble *et al.*[9] demonstrated that allowed below-horizon trajectories exist. In fig. 3, we can see one such trajectory starting at infinity and being bent by the magnetic field in a way such that its approach direction is below the local horizon. In contrast to the allowed and forbidden bands seen in fig. 2, there will be a forbidden band of rigidities starting at rigidity value R_H and going all the way up to a rigidity value of ∞ . This is shown in fig. 4 where bands of allowed and forbidden trajectories are calculated for a grid of rigidities and azimuths with a fixed zenith angle that points below the local horizon.

1.3. The PLANETOCOSMICS simulation framework

PLANETOCOSMICS is a simulation framework developed by Desorgher *et al.*[10], who state that its main applications are

- The computation of the propagation of charged particles in the planet magnetosphere
- The computation of the flux of particles resulting from the interaction of cosmic rays with the planet’s atmosphere and soil at user-defined altitudes
- The computation of the energy deposited by cosmic ray showers in the planet’s atmosphere
- The visualization of magnetic field lines and trajectories of primary and secondary particles in the planetary environment.

By default, this can be done for the Earth, Mars, and Mercury, where each planet has different models for its magnetic field and atmosphere. The code of PLANETOCOSMICS is written such that adding new models for magnetic fields or atmospheres and adding new planets is relatively simple.

According to the PLANETOCOSMICS documentation[11], the magnetic field used in the simulation is the sum of two contributions, namely the internal field resulting from sources inside the planet and the external field giving a contribution in the magnetosphere. As internal field, we are using the *International Geomagnetic Reference Field* (IGRF), a magnetic field model using so-called Gauss coefficients as input. As the documentation[11] explains, these are derived from magnetic field measurements and issued every five years by the *International Association of Geomagnetism and Aeronomy*. To obtain the

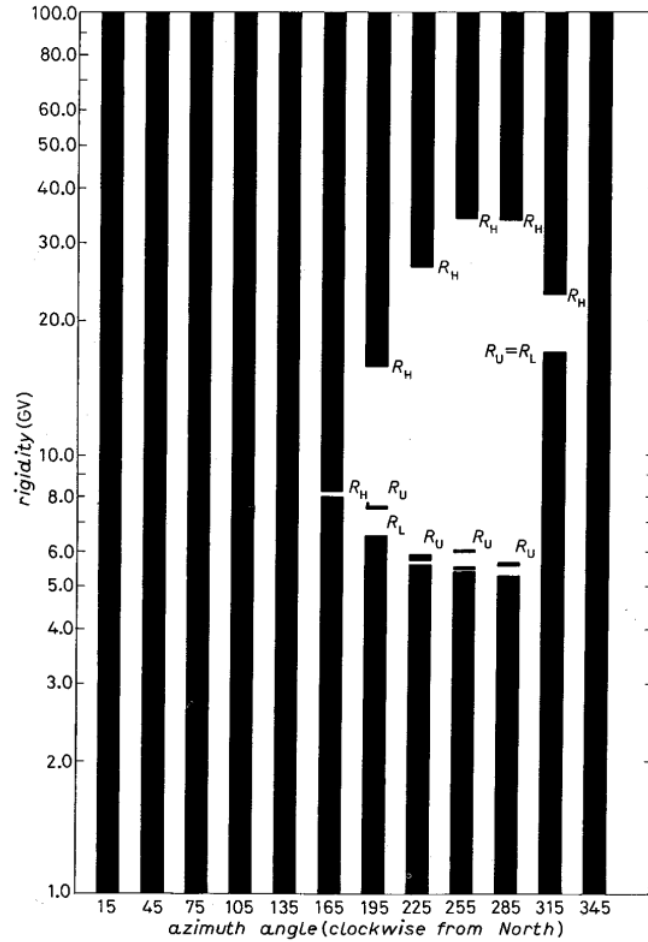


Figure 4: Allowed and forbidden rigidity bands at location 20°N , 270°E , 400 km and zenith angle 120° , which is below the local horizon. Forbidden trajectories are indicated by black and allowed ones by white. While R_U and R_L are still the highest/lowest *computed* forbidden \rightarrow allowed transitions, the rigidity R_H indicates the highest *computed* allowed \rightarrow forbidden transition. Source: Cooke *et al.*[2]

parameters for a particular point in time, one can interpolate and extrapolate them from the parameters published every five years. A table containing the Gauss coefficients from 1900 to the release year of the documentation in 2005 is distributed with the PLANETOCOSMICS code, and the reference date for the IGRF model can be given as input. As external field, we are using the model by Tsyganenko and Sitnov[12], abbreviated in the following as the TS05 model, which is not by default included in PLANETOCOSMICS. Instead, it was included by von Doetinchem and Yamashiro[1]. This model takes into account that charged particles emitted by the sun, called the solar wind, have an increasing influence on the magnetic field at higher altitudes, as described by Tsyganenko[13]. The TS05 model also needs input parameters that are updated regularly, which can be found at [14] for every year from 1995 to 2020.

PLANETOCOSMICS offers many macros to define the environment or to perform different calculations, which can be given in a macro file in the `.g4mac` format. These macros are described in the PLANETOCOSMICS documentation[11], and an example macro file written by Philip von Doetinchem is shown in appendix A. We will discuss a few macros throughout this work when their introduction is needed. For the explanation of the other macros, I will refer to the PLANETOCOSMICS documentation[11].

This concludes the introductory part of this report. The following section will discuss the first task I got assigned shortly after arriving in Hawai'i.

2. Finding the origins of the geomagnetic cutoff hotspot

2.1. Description of the original draft

The starting point of the project was an unpublished draft by von Doetinchem and Yamashiro[1] that used the PLANETOCOSMICS framework for different cutoff calculations needed to treat various problems. We will talk primarily about the cutoff calculations themselves because the main task of this project was to debug them and extend their functionality. The treatment of the problems that need these cutoff calculations is ongoing research that should remain confidential until published.

The main reason why the draft by von Doetinchem and Yamashiro[1] was not published was an unexpected and unintuitive finding that could not be explained at that time

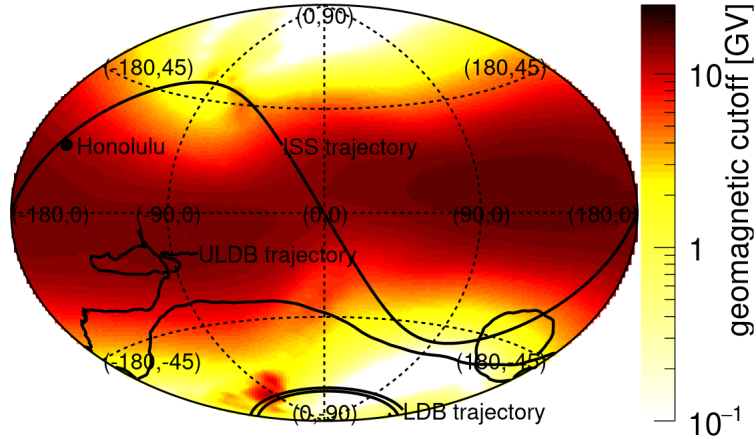


Figure 5: The average of the effective cutoff R_C over an isotropic incoming particle distribution is shown as a function of position. The particle distribution was isotropic for values of the cosine of the zenith from 0.6 to 1, and the altitude was fixed at 400 km. The magnetic field of the first day of operation of the AMS-02 experiment was simulated, i.e., on the 19th May 2011. Note the unexpected cutoff hotspot in the southern hemisphere at about -70°N , -90°W . Source: von Doetinchem and Yamashiro[1]

because of temporal constraints. This finding is a geomagnetic cutoff hotspot on the southern hemisphere that can be seen in fig. 5 at about -70°N , -90°W . In this figure, an average of the effective cutoff R_C is plotted over different positions over the entire Earth. As von Doetinchem and Yamashiro[1] explain, most detectors measuring cosmic ray particles face perpendicularly outwards from the Earth, meaning that the magnetic field component that is horizontal to the Earth's surface has the strongest influence on the particles that are measured. The geomagnetic field lines in the vicinity of the Earth are perpendicular to the Earth's surface at the poles and parallel at the equator, which can be explained by remembering that Earth's magnetic field can be modeled as a dipole field. As a consequence, we expect that the effective cutoff R_C has its maximum at the equator and decreases towards the poles. This can be seen in fig. 5 with the surprising exception of the above mentioned cutoff hotspot at -70°N , -90°W .

To investigate this phenomenon further, von Doetinchem and Yamashiro[1] plotted the region around the hotspot at time intervals of 400 days to see whether it changed its position and form. This plot is shown in fig. 6, where we can see that the position and the form of the hotspot change with time.

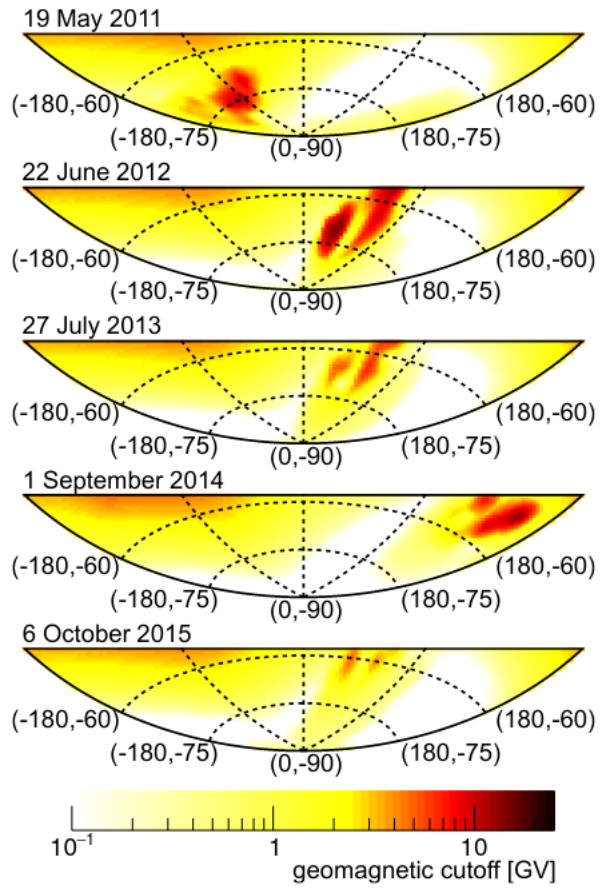


Figure 6: The average of the effective cutoff R_C is plotted analogous to fig. 5, but only in the region of the hotspot and for different times. It can be seen that the hotspot changes its position and form with time. Source: von Doetinchem and Yamashiro[1]

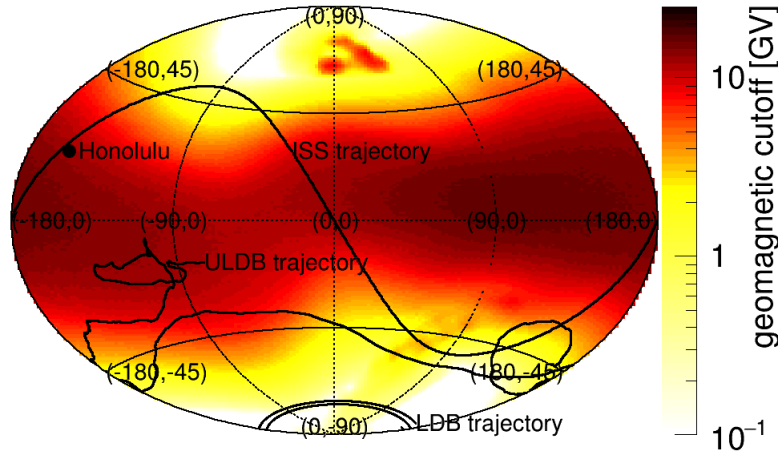


Figure 7: The average of the effective cutoff R_C is shown as a function of position analogous to fig. 5. In this plot, the reference date for the magnetic field models is the 14th January 2016. Note that the geomagnetic cutoff hotspot is now on the northern hemisphere at approximately 65°N , 0°E . Source: von Doetinchem[15]

At the beginning of this project, the origin of the hotspot was unclear. It could have been an interesting phenomenon that results from the complicated structure of the magnetic field in that region, but it could have also been a bug in the software. The first task given to me was to clarify that situation.

2.2. Determining whether the hotspot is a real phenomenon

This section focuses on determining whether the geomagnetic cutoff hotspot results from an interesting phenomenon or a bug in the software. Section 2.3 will then focus on finding the exact origin of the hotspot.

In the previous section, we looked at fig. 5, which is the original figure shown by von Doetinchem and Yamashiro[1]. It shows an average effective cutoff as a function of position for a magnetic field using the 19th May 2011 as a reference date. In this section, however, we will take a closer look at fig. 7, where the hotspot can be found in the northern hemisphere at approximately 65°N , 0°E . The reason why I chose to work with fig. 7 is that, at that time, I only had the results of the PLANETOCOSMICS calculation for that hotspot available.

To get a first clue of what is happening in the program, we should look at the program's output. As one can see at the last line of appendix A, the macro used to calculate the cutoff rigidities is

PLANETOCOS/MAGNETIC/RCutoffVsDirection.

The output will be one plaintext file for each position in which the calculated cutoff rigidities R_L , R_C , and R_U as defined in section 1.2.2 are listed for each direction. A short excerpt of the output of the PLANETOCOSMICS cutoff calculation resulting from the macro file in appendix A is shown in table 1. In order for a hotspot to exist at that point, the directions calculated at that position should have a high effective cutoff R_C . The by far highest effective cutoff in table 1 is at direction (Zenith, Azimuth) = (35°, 170°), which has the value $R_C = 98.14$ GV. If we look at the complete output, there are multiple directions which also have exactly $R_U = 100.01$ GV and an effective cutoff $R_C \geq 95$ GV. We will see later in section 3 why so many R_U have exactly that particular value. The physical intuition behind the high value of R_C for the direction (35°, 170°) can be found if one remembers the definition of R_C given in eq. (17). A high value of R_C indicates that most of the trajectories in the penumbra are forbidden.

To see whether the large R_C is the result of a bug, we could backtrace a set of particles with rigidities between $R_L = 0.2$ GV and $R_U = 100.01$ GV and visualize their trajectories. If we see that many trajectories leave the magnetosphere and are therefore allowed, we would know that there is at least one bug in the software because the effective cutoff R_C would have to be smaller in that case according to eq. (17). On the other hand, if we see a lot of forbidden trajectories, the large effective cutoff R_C could result from either a real phenomenon or a bug that could be, e.g., hidden in the magnetic field models. The backtracing can be done using PLANETOCOSMICS because one can assume with high confidence that the bug is not in the framework's backtracing algorithm. The reason for this is that PLANETOCOSMICS uses Geant4² to simulate the propagation of particles, which is, according to Allison *et al.*[16], a simulation toolkit used for at least 16 years by, among others, the LHC, ESA, and NASA. Therefore, it is highly improbable that a bug having such a high impact on the result remained undetected over such a long time.

Figure 8 visualizes the trajectory of particles with rigidities $R = 0.2$ GV, 0.3 GV, . . . , 100 GV at the above mentioned northern hotspot in the direction where $R_C = 98.14$ GV. The trajectories with the lowest rigidities, colorized in red, experience a strong bending by

²<https://geant4.web.cern.ch/>

Table 1: Excerpt of the PLANETOCOSMICS output at 65°N, 0°E using the 14th January 2016 as reference date. The angles are measured in ° and the rigidities in GV.

Zenith	Azimuth	R_U	R_C	R_L
35.00	90.00	10.38	9.48	0.19
35.00	100.00	10.28	9.31	0.19
35.00	110.00	10.23	8.79	0.19
35.00	120.00	5.93	5.03	0.19
35.00	130.00	5.52	4.72	0.19
35.00	140.00	5.20	4.57	0.20
35.00	150.00	4.96	4.25	0.20
35.00	160.00	4.80	4.00	0.20
35.00	170.00	100.01	98.14	0.20
35.00	180.00	28.65	27.46	0.20
35.00	190.00	18.22	17.26	0.20
35.00	200.00	0.20	0.20	0.20
35.00	210.00	0.21	0.21	0.21

the magnetic field. On the other hand, trajectories with higher rigidities, going from green to blue, leave the magnetosphere with trajectories that are almost straight lines. Since most of the trajectories can escape the magnetosphere without being trapped in a periodic orbit or without intersecting the Earth, it can be concluded that the high effective cutoff R_C must be the result of a bug. Since these unrealistically high effective cutoff values are used in the averaging process in fig. 7, this bug could be the source of the cutoff hotspot.

2.3. Finding the source of the bug

The search for the bug was done by using the debugger GDB to follow the control flow of the program. This procedure was a rather time-consuming step in the project, but it was also rewarding because I gained a better understanding of the PLANETOCOSMICS codebase. Throughout this section, we will discuss the result of the search instead of the search itself.

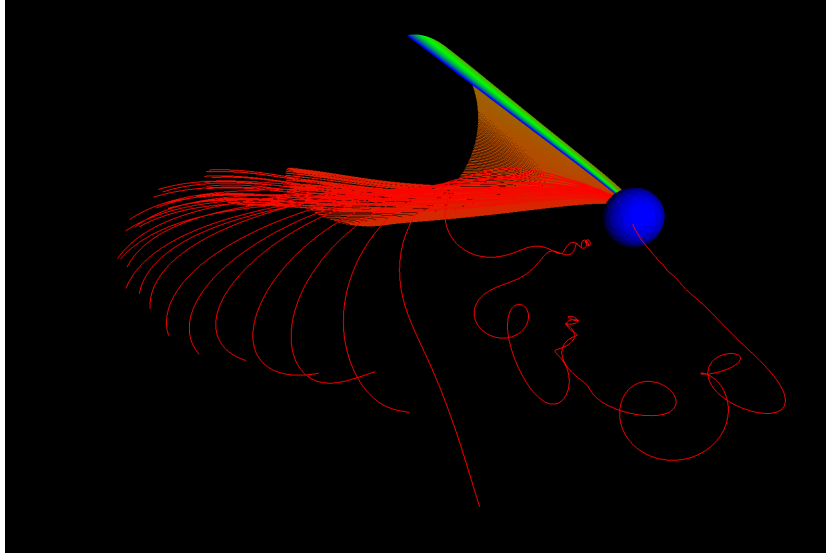


Figure 8: Particles with rigidities $R = 0.2 \text{ GV}, 0.3 \text{ GV}, \dots, 100 \text{ GV}$ are traced back in the direction $(35^\circ, 170^\circ)$ at the position of the northern hotspot in fig. 7, namely at $65^\circ\text{N}, 0^\circ\text{E}$. The color of the trajectory indicates its rigidity, starting with the lowest rigidities indicated in red and ending with the highest rigidities in blue.

The most important finding throughout the search was the notion of “termination conditions”. These are conditions used by PLANETOCOSMICS to determine whether the backtracing of a trajectory should be terminated. If the calculation terminates, the condition also decides whether the trajectory should be labeled allowed or forbidden. Examples of termination conditions are

- The function `OutsideMagnetosphere` returns true, resulting in an allowed trajectory
- The length of the trajectory is larger than, e.g., $100 \cdot R_E$, where R_E is the radius of the Earth
- The proper time of the trajectory is larger than, e.g., 100 s
- A fixed maximum value for the computation time is exceeded
- The particle orbits too many times around the planet
- The particle leaves the predefined world volume

Some termination conditions are hardcoded, but others accept input values given by macros in the macro file. The latter is true, e.g., for the maximum length or the maximum

proper time of the trajectory, that are set to be $100 \cdot R_E$ and 100 s in appendix A. It is also true for the boundaries of the world volume, which is defined to be $50 \cdot R_E$ above the atmosphere in appendix A. As it turns out, this is the root of the problem. Since particles are allowed to travel a distance up to $100 \cdot R_E$, the distance between the atmosphere and the boundary of the world volume is too small to contain all trajectories in the world volume. Unfortunately, in the case of an intersection of a trajectory with the world volume's boundary, the calculation terminates silently and labels the trajectory as forbidden. Since these trajectories describe particles far away from Earth, they would normally be classified as allowed if the termination condition was not triggered.

Hence, the source of the hotspots is not a bug in the sense of an error in the program but rather a mistake in the input macro file. Let D_{\max} be the maximum distance between the atmosphere and a position that we want to investigate in the context of cutoffs. Suppose we increase the distance between the atmosphere and the world volume above $D_{\max} + 100 \cdot R_E$. In that case, it will be impossible for the particle to intersect with the world volume since the termination condition regarding the maximum length of the trajectory would be triggered before an intersection could happen. Additionally, PLANETOCOSMICS was modified to terminate with an error if the world volume's boundary is intersected to ensure that erroneous input values are detected in the future.

In the example macro file in appendix A, we calculate particles at altitude 600 km in a model of the Earth that has no atmosphere. Therefore, the distance between the atmosphere and world volume should equal the distance between the Earth's surface and the world volume. If we change the distance between the atmosphere and world volume in appendix A to be, e.g., $101 \cdot R_E$, all trajectories will be included in the world volume. Running the cutoff calculations again leads to the results shown in table 2. If we directly compare table 1 and 2, we can see that the values in the second table are much smaller than in the first, which causes the cutoff hotspot to disappear. This behavior is expected since the cutoff calculation algorithm in the first table encountered many more trajectories that were incorrectly labeled as forbidden, which led to higher values of R_C and R_U . A more precise explanation of the latter argument will be given in the following section, where we will have a more detailed discussion of the PLANETOCOSMICS cutoff algorithm and extensions of it that will prove more suitable for us.

Table 2: Excerpt of the PLANETOCOSMICS output analogous to table 1, but with an increased distance of $101 \cdot R_E$ between the atmosphere and the world volume’s boundary. The angles are measured in $^\circ$ and the rigidities in GV.

Zenith	Azimuth	R_U	R_C	R_L
35.00	90.00	0.19	0.19	0.19
35.00	100.00	0.19	0.19	0.19
35.00	110.00	0.19	0.19	0.19
35.00	120.00	0.19	0.19	0.19
35.00	130.00	0.19	0.19	0.19
35.00	140.00	0.20	0.20	0.20
35.00	150.00	0.20	0.20	0.20
35.00	160.00	0.20	0.20	0.20
35.00	170.00	0.20	0.20	0.20
35.00	180.00	0.20	0.20	0.20
35.00	190.00	0.20	0.20	0.20
35.00	200.00	0.20	0.20	0.20
35.00	210.00	0.21	0.21	0.21

3. Extending the PLANETOCOSMICS framework

In one of the weekly meetings of Professor von Doetinchem’s working group, I presented how the PLANETOCOSMICS cutoff algorithm works in detail after I followed the program’s control flow for some time during the search for the origin of the cutoff hotspot. In the discussion that followed my presentation, we agreed that the algorithm had some properties which were unfavorable for the treatment of various problems that the group is currently working on. My next assignment was to lift these unfavorable properties by extending the algorithm.

This section will discuss the PLANETOCOSMICS cutoff algorithm and the above-mentioned unfavorable properties. This is followed by an explanation of the algorithm implemented during this project and a demonstration of the algorithm’s output. I tried out many different algorithms and approaches to implement them during the project. However, for brevity, we will focus on the final result in this section rather than on the journey towards it.

3.1. Motivation for the extension

We will start with a more detailed explanation of the macro

```
/PLANETOCOS/MAGNETIC/RCutoffVsDirection coorsys zen0 dzen nzen azim0
dazim nazim output_file.
```

that was used for the calculation of cutoffs so far. This macro performs a cutoff calculation at a position specified in the macro file for different directions \mathbf{zen}_i and \mathbf{azim}_j where $\mathbf{zen}_i = \mathbf{zen}_0 + i \cdot \mathbf{d}_{zen}$ with $i = 0, \dots, n_{zen} - 1$, and analogous for \mathbf{azim}_j . The output of this macro will be a plaintext file at the path given by the argument `output_file`, which lists the values R_L , R_C , and R_U for the different directions. For one cutoff calculation at a particular direction, the macro executes the following algorithm:

1. Calculate the Størmer cutoff R_S in a dipole approximation. The formula for this can be found, e.g., in Cooke *et al.*[2].
2. Set the minimum and maximum rigidity to be considered with $R_{\min} = 0.01$ GV and $R_{\max} = \max(100 \text{ GV}, R_S + 10 \text{ GV})$.
3. Check whether $R = R_S$ yields an allowed trajectory. If not, increment R by 1 GV until an allowed trajectory is found. Call the corresponding rigidity R_{allowed} .
4. Decrement $R = R_{\text{allowed}}$ by 0.01 GV until a forbidden trajectory is found. Call it $R_{\text{forbidden}}$. If $R < 0.015$ GV during the search, then return that R_L , R_C and R_U are all 0 GV. If $R < R_{\min} + 0.01$ GV, then return that R_L , R_C and R_U have value R .
5. Increment $R = R_{\text{allowed}}$ by 0.01 GV and count the allowed trajectories. If 100 allowed trajectories in a row are found, i.e., an allowed 1 GV band, then R_U is defined to be the smallest allowed rigidity of that band. If $R > R_{\max} - 0.01$ GV during the search, R_U is defined to be the rigidity of the smallest allowed trajectory of the current allowed band. If the last calculated rigidity was $R = R_{\max} = 100$ GV and if that trajectory was forbidden, R_U will be set to 100.01 GV.
6. Decrement $R = R_{\text{forbidden}}$ by 0.01 GV and count the forbidden trajectories. If 100 forbidden trajectories in a row are found, then R_L is the last found allowed rigidity. If $R < R_{\min} + 0.01$ GV during the search, R_L is the last found allowed rigidity.
7. Count during the previous steps how many allowed trajectories n_{allowed} are between $R_L - 0.01$ GV and R_U . Then, calculate $R_C = R_U - n_{\text{allowed}} \cdot 0.01$ GV. Return R_L ,

R_C and R_U .

With this detailed understanding of the algorithm, we can give a more precise explanation of why the intersection with the world volume’s boundary in section 2.3 led to cutoff hotspots. The main problem happens in step 5 of the algorithm. There, the probed rigidity is incremented until either a band of allowed trajectories is found or the maximum rigidity R_{\max} is reached. If these probed rigidities lead to trajectories that intersect with the world volume’s boundary, it is unlikely that a 1 GV band of allowed trajectories can be found because all trajectories are labeled as forbidden due to the intersection. Therefore, the last calculated rigidity will be $R = 100$ GV, which will be labeled as forbidden due to the intersection with the world volume’s boundary, leading to $R_U = 100.01$ GV according to step 5 of the algorithm. This value can be seen for the direction (Zenith, Azimuth) = $(35^\circ, 170^\circ)$ in the R_U column of table 1, and it can also be encountered at many other directions in the full PLANETOCOSMICS output. Since these directions lead to high values of R_U and a penumbra that has a lot of wrongly labeled forbidden trajectories, the effective cutoff values of these directions will be large according to eq. (17), which in turn leads to the cutoff hotspot in fig. 7.

The algorithm described above has some advantageous properties that we do not want to lose when we construct our new algorithm. The fact that the algorithm starts by calculating the Størmer cutoff R_S and takes it as a first guess is expected to save computing time if we are in the vicinity of the Earth where the magnetic field is approximately a dipole field. Another positive aspect is that the search in each direction of the rigidity band is terminated by the finding of a 1 GV rigidity band, which enhances the probability that the whole penumbra got discovered during the calculation. On the other hand, as mentioned above, our working group also discussed some suboptimal aspects of the algorithm.

The first negative aspect is that the macro only allows to sample directions that are uniformly spaced in their zenith angles. Sampling the spherical coordinates (θ, φ) with position vector

$$\vec{\mathbf{r}} = \begin{pmatrix} \sin \theta \cos \varphi \\ \sin \theta \sin \varphi \\ \cos \theta \end{pmatrix} \quad (18)$$

uniformly leads to an undersampling at the equator and to an oversampling at the poles, which can be seen if one looks at the surface element $dA = \sin \theta \, d\theta \, d\varphi$. Because of the

$\sin \theta$ term, the surface element is small around the poles ($\theta = 0^\circ, 180^\circ$) and large around the equator ($\theta = 90^\circ$), and uniform sampling of the coordinates (θ, φ) therefore leads to a higher density of points on the poles compared to on the equator. If one wants a set of coordinates that can be uniformly sampled such that the sphere is covered uniformly with points, one should use the coordinates $(\cos \theta, \varphi)$. This can be seen if one looks at the integration of the surface element dA over the sphere, i.e.,

$$\frac{1}{4\pi} \int_0^{2\pi} d\varphi \int_0^\pi d\theta \sin \theta = 1. \quad (19)$$

The integrand $f(\theta) = \frac{1}{4\pi} \sin \theta$ can be understood as a probability density determining how probable it is that a point is sampled in a particular region on the sphere. With this probability density, the probability that a point is in a certain region on the sphere is equal to the fraction of the surface area of that region and the whole surface area of the sphere, which leads to uniform sampling on the sphere. If we look at the integral of the θ coordinate in eq. (19), we can perform a change of coordinates from θ to $\cos \theta$ by doing

$$\int_0^\pi \sin \theta d\theta = \int_{-1}^1 d(\cos \theta). \quad (20)$$

In these coordinates $(\cos \theta, \varphi)$, the probability density is just $\frac{1}{4\pi}$, which is constant over the whole sphere. Therefore, uniform sampling of the coordinates $(\cos \theta, \varphi)$ leads to a uniform distribution of points on the sphere, and we should make sure that we use these coordinates in our new cutoff algorithm.

The second unfavorable property of the cutoff algorithm is that the rigidity interval is probed uniformly on the whole interval. As we can see from the description of the cutoff algorithm above, rigidities are selected in intervals of 0.01 GV, regardless of whether we are probing small rigidities of order $\mathcal{O}(0.1 \text{ GV})$ or larger rigidities of order $\mathcal{O}(10 \text{ GV})$. We prefer a logarithmic sampling of rigidities such that each order of magnitude has an equal number of probed rigidities, meaning that smaller orders or magnitudes are sampled finer than larger ones.

The last negative aspect that we will discuss is the output format of the algorithm. At the moment, the output for each direction consists of the three rigidities R_L , R_C , and R_U . This output format wastes a large amount of information that was computed during the cutoff calculation, especially information about the structure of the penumbra since the whole penumbra was probed in rigidity intervals of 0.01 GV. This information

is not completely lost since the effective cutoff R_C is computed with it, but, e.g., the information about the structure of the bands in the penumbra is lost completely. It would be favorable if the algorithm's output would store this information in more detail, e.g., in a histogram.

3.2. Sketching the new algorithm

In the last section, we mentioned three different properties that the working group considered suboptimal for their purposes and that should be lifted by implementing a new algorithm. The first point regarding the usage of the coordinates $(\cos\theta, \varphi)$ is rather easy to fix by just changing the input parameters of the macro regarding the zenith angle, namely \mathbf{zen}_0 , $\mathbf{d}_{\mathbf{zen}}$, and $\mathbf{n}_{\mathbf{zen}}$, to $\mathbf{cos}(\mathbf{zen})_0$, $\mathbf{d}_{\mathbf{cos}(\mathbf{zen})}$, and $\mathbf{n}_{\mathbf{cos}(\mathbf{zen})}$. This means that directions will be sampled with coordinates $\mathbf{cos}(\mathbf{zen})_{\mathbf{i}} = \mathbf{cos}(\mathbf{zen})_0 + \mathbf{i} \cdot \mathbf{d}_{\mathbf{cos}(\mathbf{zen})}$ with $\mathbf{i} = 0, \dots, \mathbf{n}_{\mathbf{cos}(\mathbf{zen})} - 1$, which leads to uniform sampling on the sphere as described in section 3.1.

Analogous to the old algorithm, we will fix a minimum rigidity R_{\min} and a maximum rigidity R_{\max} that can be selected by the user and that give us the boundaries of a rigidity interval. To save computing time, these boundaries should be chosen such that they only include the rigidities which are physically relevant for the task at hand. In order to deal with the second negative aspect of the old algorithm, we will consider this interval to be logarithmic, meaning that the lower and upper boundary are $\log(R_{\min})$ and $\log(R_{\max})$, respectively. To be precise, one would have to write $\log(R_{\min} \text{ GV}^{-1})$ and $\log(R_{\max} \text{ GV}^{-1})$, but we will omit this level of notational detail in the following. The third negative aspect discussed in section 3.1 will be solved by choosing the histogram class TH1D of the data analysis framework ROOT³ to represent the computed data. This data structure has the advantage that arithmetical operations can be performed on multiple histograms if they have the same bin edges, which will be of great use to calculate, e.g., averages over multiple directions or positions. To make sure that all histograms have the same bin edges, we will cover the logarithmic interval with n_{bins} bins. Since the interval has length $d = \log(R_{\max}) - \log(R_{\min}) = \log(R_{\max}/R_{\min})$, the bin width of each bin will be d/n_{bins} . This means that the logarithm of bin edge E_i is described by

$$\log(E_i) = \log(R_{\min}) + i \cdot \frac{d}{n_{\text{bins}}}, \quad (21)$$

³<https://root.cern/>

where $i = 0, \dots, n_{\text{bins}}$. This can be exponentiated to obtain

$$E_i = R_{\min} \cdot \left(\frac{R_{\max}}{R_{\min}} \right)^{i/n_{\text{bins}}}. \quad (22)$$

The algorithm that will be presented below will decide on what bins should be calculated. The phrase ‘‘calculating a bin’’ means that m rigidities in the bin will be selected and traced back. The selection is done uniformly on the logarithmic interval. If we define the rigidity $R_{i,j}$ to be the j th probed rigidity in the i th bin, then we can calculate $\log(R_{i,j})$ by

$$\log(R_{i,j}) = \log(E_i) + j \cdot \frac{d}{n_{\text{bins}} \cdot m} = \log(R_{\min}) + \left(i + \frac{j}{m} \right) \cdot \frac{d}{n_{\text{bins}}} \quad (23)$$

with $j = 0, \dots, m-1$. Hence, after exponentiation, one obtains eq. (22) with $i \rightarrow (i + \frac{j}{m})$. If $R_{i,j}$ is found to be forbidden after backtracing its trajectory, the height of bin i will be increased by $1/m$, otherwise the bin’s height will not change. Therefore, the height of a bin will approximate the probability that a trajectory with a rigidity belonging to that bin will be forbidden. The algorithm that selects the bins to be calculated works as follows:

1. Calculate the Størmer rigidity R_S and find the bin that it belongs to. Calculate that bin.
2. Go one bin to the right and calculate it. Repeat that until k bins in a row are found that have height zero, i.e., that only consist of allowed trajectories, or until R_{\max} is reached. All bins to the right of the last calculated bin are assumed to have zero height.
3. Go back to the Størmer bin. Go one bin to the left and calculate it. Repeat that until k bins in a row are found that have height one, or until R_{\min} is reached. All bins to the left of the last calculated bin are assumed to have a height of one.

3.3. The syntax of the new macro

The old macro described in section 3.1 did not have input arguments to specify the position of the cutoff calculation because this could be done, according to the PLANETOCOSMICS documentation[11], with another macro,

```

/PLANETOCOS/SOURCE/SetPosition coorsys altitude length_unit latitude
longitude angle_unit,

```

where `coorsys` describes the used coordinate system. The meaning of the other input arguments should be self-explanatory. Contrary to that, our new macro will have input arguments that specify the position of the cutoff calculation. We will also make a coordinate change by substituting the latitude with the sine of the latitude. The reason for this is analogous to the discussion of the $\cos\theta$ coordinate in section 3.1, but we need to use a sine here because the latitude is a coordinate with values in the range $(-90^\circ, 90^\circ)$, while the zenith angle has values in the range $(0^\circ, 180^\circ)$. This will make the process of sampling positions on the sphere easier. Note that each macro file calculates the cutoff histograms at only one position, but for multiple directions at that position. This makes it possible to calculate the cutoff histograms at different positions in parallel without having to deal with parallelization at the coding level. The syntax of our new macro is

```

/PLANETOCOS/MAGNETIC/isForbiddenVsRigidityVsDirection
altitude sin(latitude) longitude
cos(zen)_0 d_cos(zen) n_cos(zen)
azim_0 d_azim n_azim
/path/to/directory AlgorithmID,

```

where `/path/to/directory` is a path to a directory in which the results will be saved, and `AlgorithmID` is an identifier for the algorithm. The latter was necessary because I experimented with different algorithms which were uniquely identified by that argument. The algorithm described in section 3.2 has the identifier `HistsOnFlexibleRange`. All the other input arguments are either self-explanatory or analogous to the ones in section 3.1.

3.4. Examples of cutoff histograms

In the last section, we will look at some examples of cutoff histograms. The histograms span an rigidity interval from $R_{\min} = 0.1 \text{ GV}$ to $R_{\max} = 100 \text{ GV}$. This interval is divided in $n_{\text{bins}} = 150$ bins, and the number of allowed/forbidden bins in a row that need to be found is set to $k = 7$. We will look at three different histograms from three different positions, but they share the altitude of 600 km and the same direction (Zenith, Azimuth) = $(35^\circ, 170^\circ)$, which is the direction that led to wrong results at the hotspot in section 2.2. The reference date for the magnetic field is the 14th January

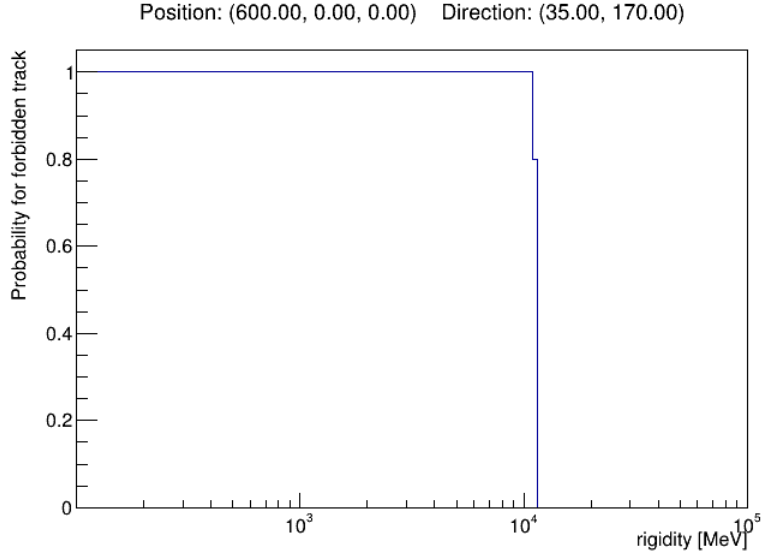


Figure 9: A cutoff histogram at position 0°N , 0°E on the equator.

2016, which is the exact date where the hotspot was calculated in section 2.2.

The first position that we will inspect is the point 0°N , 0°E , which is on the equator. The cutoff histogram can be seen in fig. 9. We can see that the penumbra is a relatively small interval at this combination of position and direction because it is fully included in one bin. The cutoffs are relatively high compared to the other histograms in this section that were calculated further north. As discussed in section 2.1, this is expected because the magnetic field lines are horizontal at the equator in the dipole approximation, leading to more shielding from particles with small zenith angles. The second position is further to the north at 40°N , 0°E . We can see the corresponding cutoff histogram in fig. 10. The structure of its penumbra is much more complex than the previous cutoff histogram at the north pole. The last position is again further north at 65°N , 0°E , which is exactly the position and direction combination that led to a large effective cutoff R_C in table 1. We can see the cutoff histogram in fig. 11. The larger end of the penumbra is a little bit below 0.2 GV which is the value for R_U in table 2. While the old algorithm did not calculate values below 0.2 GV and simply set $R_L = R_C = R_U$, our algorithm calculated the penumbral structure in more detail there because we chose to calculate until $R_{\min} = 0.1$ GV is reached and because we have finer sampling since we treat the rigidity axis as logarithmic.

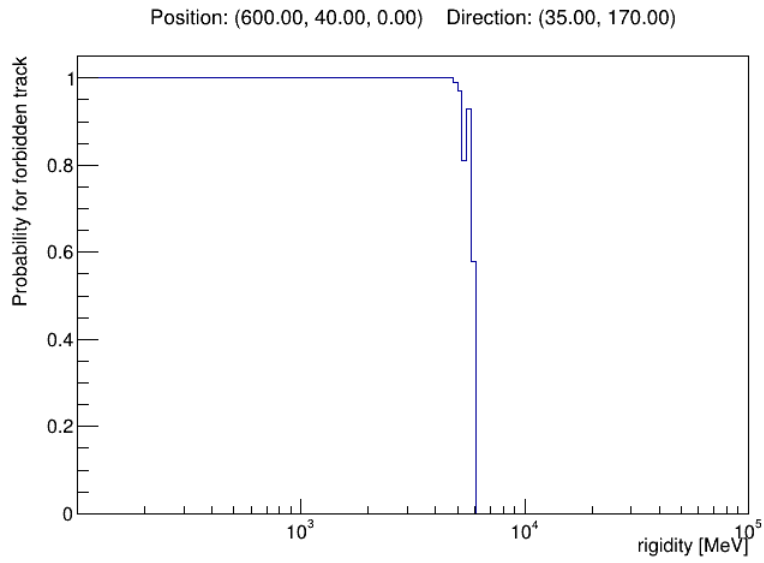


Figure 10: A cutoff histogram at position 40 °N, 0 °E.

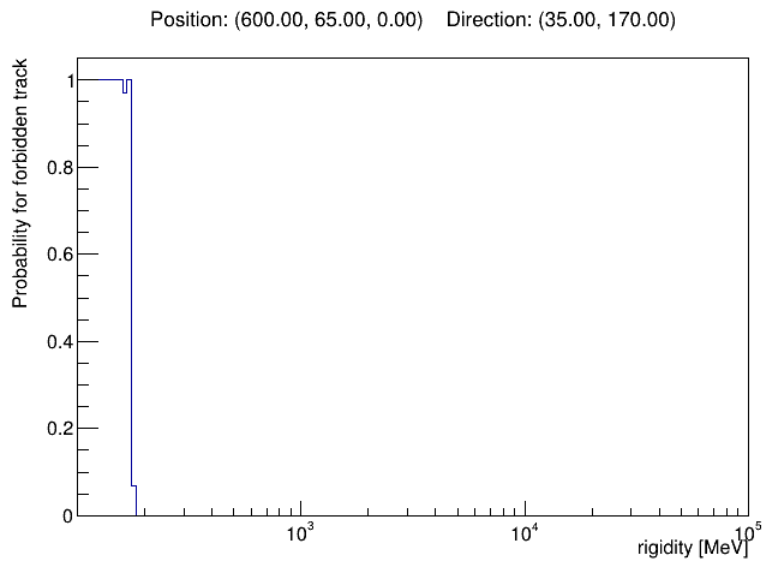


Figure 11: A cutoff histogram at position 65 °N, 0 °E, the location of the hotspot in fig. 7.

4. Summary and results

This work began with a short introduction of the rigidity as a physical quantity followed by a discussion of the history and the terminology used in the context of the access problem, which was a summary of the paper written by Cooke *et al.*[2]. The treatment of this problem can be divided into two periods. The first period focused on theoretical considerations, while the second one used digital computers to better understand the access of charged particles to points in the magnetosphere. The notion of cutoff rigidities was defined, and some basic functionality of the PLANETOCOSMICS framework, which can be used to calculate those cutoffs, was introduced.

Section 2 discussed some aspects of the unpublished draft by von Doetinchem and Yamashiro[1] that served as a starting point for the project. One of the findings in the draft was the appearance of cutoff hotspots, which were regions with a high effective cutoff R_C located relatively close to the Earth's poles. These hotspots were unexpected and unintuitive because the magnetic field lines at the poles are not as horizontal to Earth's surface as they are close to the equator. Since most detectors face radially outwards from the Earth, we are primarily interested in particles with small zenith angles. These are influenced strongly by the magnetic field component that is horizontal with respect to Earth's surface. Therefore one would expect high cutoffs at the equator that decrease if one moves towards the poles. Whether the hotspots result from a real phenomenon or a problem with the software was solved by visualizing the trajectories of particles that were traced back starting in a cutoff hotspot region. Most of the trajectories were allowed, while the program's output pointed towards a majority of forbidden trajectories. This contradiction showed that there must be at least one problem with the software. After some careful debugging sessions, the problem was identified to be a mistake regarding the size of the world volume in the input scripts of PLANETOCOSMICS.

Section 3 explained the cutoff algorithm of PLANETOCOSMICS in more detail and highlighted some of its advantages and disadvantages. Based on this discussion, a new algorithm was proposed that computes cutoff histograms. These histograms store much more information than the standard output format of PLANETOCOSMICS, which compresses all computed information into only three rigidities R_L , R_C , and R_U . This was followed by an explanation of the syntax of the new PLANETOCOSMICS macro. In the end, some example histograms calculated at different points in the magnetosphere were shown and discussed.

References

- [1] P. v. Doetinchem and B. Yamashiro, “Geomagnetic Cutoff Calculations for the Interpretation of Low-rigidity Cosmic-ray Antiparticle Measurements,” unpublished draft, 2017.
- [2] D. J. Cooke, J. E. Humble, M. A. Shea, *et al.*, “On cosmic-ray cut-off terminology,” *Il Nuovo Cimento C*, vol. 14, no. 3, pp. 213–234, May 1991, ISSN: 0390-5551. DOI: 10.1007/BF02509357. [Online]. Available: <https://doi.org/10.1007/BF02509357>.
- [3] C. Störmer, “Periodische Elektronenbahnen im Felde eines Elementarmagneten und ihre Anwendung auf Brüches Modellversuche und auf Eschenhagens Elementarwellen des Erdmagnetismus. Mit 32 Abbildungen.,” *Zeitschrift für Astrophysik*, vol. 1, p. 237, Jan. 1930.
- [4] L. Bouckaert, “Trajectoires voisines de l’équateur,” *Ann. Soc. Sci. Brux*, vol. 54, pp. 174–193, 1934.
- [5] G. Lemaitre, M. S. Vallarta, and L. Bouckaert, “On the north-south asymmetry of cosmic radiation,” *Physical Review*, vol. 47, no. 6, p. 434, 1935.
- [6] G. Lemaitre and M. Vallarta, “On the geomagnetic analysis of cosmic radiation,” *Physical Review*, vol. 49, no. 10, p. 719, 1936.
- [7] G. Lemaitre and M. Vallarta, “On the allowed cone of cosmic radiation,” *Physical Review*, vol. 50, no. 6, p. 493, 1936.
- [8] C. Störmer, *The polar aurora*. Clarendon Press, 1955.
- [9] J. E. Humble, D. F. Smart, and M. A. Shea, “Cosmic ray access to earth satellites from below-horizon directions,” in *International Cosmic Ray Conference*, vol. 10, Jan. 1981, pp. 270–273. [Online]. Available: <https://ui.adsabs.harvard.edu/abs/1981ICRC...10..270H>.
- [10] L. Desorgher, E. Flückiger, and M. Gurtner, “The Planetocosmics Geant4 application,” *36th COSPAR Scientific Assembly*, vol. 36, Jan. 2006.
- [11] L. Desorgher. “PLANETOCOSMICS Software User Manual.” (2005), [Online]. Available: http://cosray.unibe.ch/~laurent/planetocosmics/doc/planetocosmics_sum.pdf (visited on 05/24/2022).

- [12] N. A. Tsyganenko and M. I. Sitnov, “Modeling the dynamics of the inner magnetosphere during strong geomagnetic storms,” *Journal of Geophysical Research: Space Physics*, vol. 110, no. A3, 2005. DOI: <https://doi.org/10.1029/2004JA010798>. eprint: <https://agupubs.onlinelibrary.wiley.com/doi/pdf/10.1029/2004JA010798>. [Online]. Available: <https://agupubs.onlinelibrary.wiley.com/doi/abs/10.1029/2004JA010798>.
- [13] N. A. Tsyganenko. “Modeling the Earth’s Magnetosphere Using Spacecraft Magnetometer Data.” (2021), [Online]. Available: <https://geo.phys.spbu.ru/~tsyganenko/empirical-models/> (visited on 05/24/2022).
- [14] N. A. Tsyganenko. “TS05 magnetic field model.” (2021), [Online]. Available: https://geo.phys.spbu.ru/~tsyganenko/empirical-models/magnetic_field/ts05 (visited on 05/24/2022).
- [15] P. von Doetinchem, Private Communication, 2021.
- [16] J. Allison, K. Amako, J. Apostolakis, *et al.*, “Recent developments in Geant4,” *Nuclear Instruments and Methods in Physics Research Section A: Accelerators, Spectrometers, Detectors and Associated Equipment*, vol. 835, pp. 186–225, 2016, ISSN: 0168-9002. DOI: <https://doi.org/10.1016/j.nima.2016.06.125>. [Online]. Available: <https://www.sciencedirect.com/science/article/pii/S0168900216306957>.

Appendix

A. Example macro file for PLANETOCOSMICS

```
#####
#                                                                 #
# Simulation of cosmic rays in the magentic field and          #
# atmosphere. Use of spectra produced by GALPROP                #
# Author: Philip v. Doetinchem                                  #
#                                                                 #
#####
```

```

# general control -----

/tracking/verbose 0
/control/verbose 1
/tracking/storeTrajectory 1
/vis/scene/endOfEventAction accumulate

# define atmosphere -----

/PLANETOCOS/GEOMETRY/SetHeightOfWorldAboveAtmosphere 50. rplanet
/PLANETOCOS/GEOMETRY/SetConsiderAtmosphere false

# Physics -----

/PLANETOCOS/PHYSICS/SelectTypeOfEMPhysics NONE
/PLANETOCOS/PHYSICS/SelectTypeOfHadronicPhysics NOHADRONIC
/PLANETOCOS/PHYSICS/SelectTypeOfIonHadronicPhysics NONE
/PLANETOCOS/PHYSICS/ConsiderElectromagneticNuclearPhysics false

# Initialize Geometry and Physics -----

/PLANETOCOS/Initialise

# B-Field -----

/PLANETOCOS/BFIELD/SwitchOn
/PLANETOCOS/BFIELD/SetStartDate 2016 1 14 0 0 0
/PLANETOCOS/BFIELD/SetInternalFieldModel IGRF
/PLANETOCOS/BFIELD/SetExternalFieldModel TSY2004
/PLANETOCOS/BFIELD/SetPdyn 1.33
/PLANETOCOS/BFIELD/SetTiltAngle -0.4125
/PLANETOCOS/BFIELD/SetDst -4 nT
/PLANETOCOS/BFIELD/SetImfBy -1.75 nT
/PLANETOCOS/BFIELD/SetImfBz -1.77 nT

```

```

/PLANETOCOS/BFIELD/SetW1 0.18
/PLANETOCOS/BFIELD/SetW2 0.15
/PLANETOCOS/BFIELD/SetW3 0.21
/PLANETOCOS/BFIELD/SetW4 0.13
/PLANETOCOS/BFIELD/SetW5 0.34
/PLANETOCOS/BFIELD/SetW6 0.31
/PLANETOCOS/BFIELD/PrintTSY2004Parameters

/PLANETOCOS/USERLIMIT/SetMagnetoMaxStepLength .1 rplanet
/PLANETOCOS/STOPCONDITION/SetMaxTrackLength 100. rplanet
/PLANETOCOS/STOPCONDITION/SetMaxTrackDuration 100. second
/PLANETOCOS/INTEGRATION/SetPrecision 1e-5
/PLANETOCOS/INTEGRATION/SetG4MaxStep 5e-1 rplanet
/PLANETOCOS/INTEGRATION/SetDeltaIntersection .5 km

# Compute rigidity cutoff -----

/gps/particle anti_proton

/PLANETOCOS/MAGNETIC/ResetRigidityVector
/PLANETOCOS/MAGNETIC/SetDefaultRigidityVector

/PLANETOCOS/SOURCE/SetPosition GEODETTIC 600. km 65 0 degree
/PLANETOCOS/MAGNETIC/RCutoffVsDirection GEODETTIC 0. 5. 19 0. 10. 36 /path/to
/results/CutoffVsDirection_anti_proton_0_0.dat

```